Spin-gapless semiconducting nature of Co-rich $Co_{1+x}Fe_{1-x}CrGa$

Deepika Rani,[1] Enamullah,[1] Lakhan Bainsla,[1,2] K. G. Suresh,[1] and Aftab Alam[1,*]
[1]*Department of Physics, Indian Institute of Technology Bombay, Powai, Mumbai 400076, Maharashtra, India*
[2]*WPI Advanced Institute for Materials Research, Tohoku University, Sendai 980-8577, Japan*

(Received 30 November 2018; revised manuscript received 20 February 2019; published 25 March 2019)

Spin gapless semiconductors (SGSs) are an interesting class of materials which bridge the gap between semiconductors and half-metallic ferromagnets. This class of materials shows band gap in one of the spin channels and a zero band gap in the other, and thus promote tunable spin transport. Here, we present structural, electronic, magnetic, and transport properties of Co-rich SGS $Co_{1+x}Fe_{1-x}CrGa$ using both theoretical and experimental techniques. The key advantage of Co-rich samples $Co_{1+x}Fe_{1-x}CrGa$ is the high Curie temperature (T_C) and magnetization, without compromising the SGS nature (up to $x = 0.4$), and hence our choice. The quaternary Heusler alloys $Co_{1+x}Fe_{1-x}CrGa$ ($x = 0.1$ to 0.5) are found to crystallize in LiMgPdSn-type structures having space group $F\bar{4}3m$ (number of 216). The measured Curie temperature increases from 690 K ($x = 0$) to 870 K ($x = 0.5$). The obtained T_C for $x = 0.3$ (790 K) is found to be the highest among all previously reported SGS materials. Observed magnetization values follow the Slater-Pauling rule. Measured electrical resistivity, in the temperature range of 5–350 K, suggests that the alloys retain the SGS behavior up to $x = 0.4$, beyond which it reflects metallic character. Unlike conventional semiconductors, the conductivity value (σ_{xx}) at 300 K lies in the range of 2289 S cm^{-1} to 3294 S cm^{-1}, which is close to that of other reported SGS materials. The anomalous Hall effect is comparatively low. The intrinsic contribution to the anomalous Hall conductivity increases with x, which can be correlated with the enhancement in chemical order. The anomalous Hall coefficient is found to increase from 38 S/cm for $x = 0.1$ to 43 S/cm for 0.3. Seebeck coefficients turn out to be vanishingly small below 300 K, another signature for being SGS. All the alloys (for different x) are found to be both chemically and thermally stable. Simulated magnetization agrees fairly with the experiment. As such, Co-rich CoFeCrGa is a promising candidate for room temperature spintronic applications, with enhanced T_C, magnetic properties, and SGS nature.

DOI: 10.1103/PhysRevB.99.104429

I. INTRODUCTION

In recent years, an interesting class of materials known as spin gapless semiconductors (SGSs) has attracted a lot of attention due to their peculiar electronic structure and potential applications in spintronic devices. SGS materials exhibit a finite band gap for one spin channel and a closed gap for the other spin [1]. These materials can be regarded as a combination of half-metallic (HM) ferromagnets and gapless semiconductors. This feature results in peculiar transport properties and applications in the field of spintronics since the conducting carriers (electrons or holes) are not only completely spin polarized but also easily excited due to the gapless nature in one of the spin bands. Also, mobility of carriers in this class of materials is considerably higher than that of conventional semiconductors. The schematic representation of a half-metal, gapless semiconductor and SGS is shown in Fig. 1. SGS behavior was predicted in dilute magnetic semiconductor (DMS) $PbPdO_2$ by first-principles calculations [2]. However, one of the major drawbacks of DMS is the low Curie temperature (T_C) [3]. Heusler alloy-based SGS systems have advantages over DMSs and other reported magnetic semiconductors. They have stable structure, high T_C, and high spin polarization, which make them suitable for applications in the field of spintronics. SGS behavior has been identified theoretically in many Heusler alloys [4–7] but only a few have been confirmed experimentally [8–11].

SGS behavior was verified in the equiatomic Heusler alloy CoFeCrGa (CFCG) [8]. This alloy was found to crystallize in cubic Heusler structure (LiMgPdSn prototype) with DO_3 disorder with lattice parameter of 5.79 Å. The saturation magnetization was found to be 2.1 μ_B/f.u. at 8 K. One of the methods to design materials in Heusler alloys XX′YZ is by exchanging the elements X, X′, Y, and Z or by substituting them by other elements. We have substituted Co for Fe in CFCG with the objective of improving its properties such as the band gap, Curie temperature, and spin polarization, while trying to retain the SGS nature. This is because stable materials with large band gap, high spin polarization, and high Curie temperature are desired for spintronic applications. We have synthesized $Co_{1+x}Fe_{1-x}CrGa$ ($x = 0.1$ to 0.5) alloys and studied their structural, electronic, magnetic, and transport properties. We found that all the alloys crystallize in cubic Heusler structure and the magnetization increases with excess Co and are in close agreement with the Slater-Pauling rule, a prerequisite for spintronic materials. Also, the Curie temperature of all the alloys is well above the room temperature. The alloys with $x = 0.1$ to 0.4 retain SGS nature whereas, it becomes HM at $x = 0.5$, as indicated by the resistivity data. The extrinsic and intrinsic contributions are separated in Hall resistivity. The intrinsic contribution is found to increase with

*aftab@iitb.ac.in

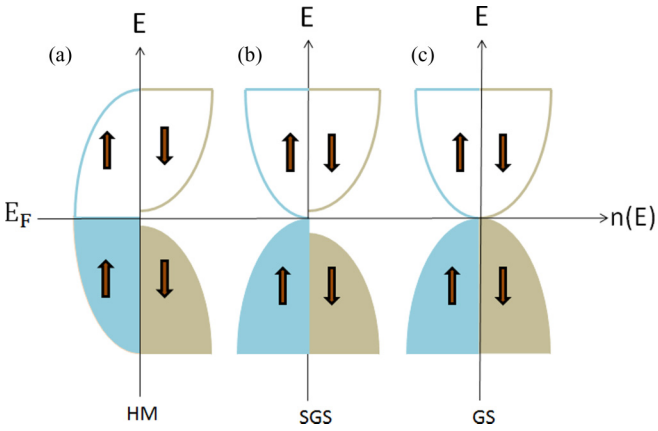

FIG. 1. Schematic representation of density of states of (a) half-metal (b) spin-gapless semiconductor, and (c) gapless semiconductor.

x and is correlated with the improved chemical order within the lattice. The extrinsic contribution is found to be negative and thus contributes to the anomalous Hall effect (AHE) in the opposite way as the Karplus-Luttinger term (intrinsic contribution) contributes. The conductivity value (σ_{xx}) at 300 K lies in the range of 2289 S cm^{-1} to 3294 S cm^{-1}, which is close to that of other reported SGS materials. The negligible Seebeck coefficient along with the conductivity behavior supports the SGS nature. Thus, the spin-gapless semiconducting nature of CoFeCrGa alloy is robust against the substitution of Co by Fe up to $x = 0.4$.

II. EXPERIMENTAL DETAILS

A. Sample synthesis

Polycrystalline samples of $Co_{1+x}Fe_{1-x}CrGa$ (2 gm) were synthesized by arc melting in the respective stoichiometric amounts of constituent elements (with at least 99.9% purity) in water-cooled copper hearth under high purity argon atmosphere. To further reduce the contamination, a Ti ingot was used as the oxygen getter. To ensure homogeneity, the ingot formed was melted several times after flipping. After melting, the samples were sealed in a quartz tube and annealed for seven days at 1073 K, followed by furnace cooling.

B. Characterization

To determine the crystal structure of the alloys, x-ray diffraction (XRD) pattern was taken at room temperature using Xpert pro diffractometer with Cu-Kα radiation. Synchrotron-based powder XRD measurements are carried out on powder samples at the extreme conditions angle dispersive and energy dispersive XRD beamline (BL-11) at the Indus-2 synchrotron source, Raja Ramanna Centre for Advanced Technology, Indore, India. Measurements are carried out in transmission geometry. The desired wavelength for ADXRD experiments is selected from the white light from the bending magnet using a Si(111) channel-cut monochromator. The monochromatic beam is then focused onto the sample with a Kirkpatrick-Baez mirror. A MAR345 image plate detector (which is an area detector) is used to collect 2D diffraction data. The sample to detector distance and the wave length of the beam are calibrated using NIST standards LaB_6 and CeO_2. Calibration and conversion/integration of 2D diffraction data to 1D, intensity vs 2θ plot, are carried out using FIT2D software [12], an arbitrary threshold mask is used to reduce the orientation effects in the measurements. XRD analysis was done with the help of FullProf suite [13], which exploits the least-squares refinement between the experimental and calculated intensities.

Magnetization isotherms at 5 K were obtained using a vibrating sample magnetometer (VSM) attached to the physical property measurement system (PPMS) (Quantum Design) for fields up to 50 kOe. Thermomagnetic curves in the high temperature region (300 K−950 K) were obtained using a VSM attached with high temperature oven, under a field of 500 Oe. Resistivity measurements were carried out using a physical property measurement system (PPMS; Quantum Design) using the linear four probe method, applying a current of 5 mA. Hall measurement was performed using the PPMS with a five-probe method by applying a current of 150 mA.

III. COMPUTATIONAL DETAILS

Electronic structure of the alloy, $Co_{1+x}Fe_{1-x}CrGa$ for $x = 0.0, 0.125, 0.25, 0.375$, and 0.50 has been simulated using density functional theory [14] implemented in Vienna *Ab initio* Simulation Package [15–17] with a projected augmented wave basis [18]. To achieve the concentration x close to the experiment, we made a symmetric $2 \times 2 \times 2$ supercell of the primitive cell. The generalized gradient approximations along with the Perdew-Burke-Ernzerhof [19] is adopted for the electronic exchange and correlation functional. A plane-wave energy cutoff of 500 eV is used with the energy convergence of 10^{-6} eV/cell. For Brillouin zone integration, $12 \times 12 \times 12$ k-points and accurate precession along with the conjugate gradient algorithm are used.

The lattice dynamics of the alloys has been analyzed using phonon frequencies calculated within the framework of density functional perturbation theory (DFPT) [20,21]. We generate the displaced atomic supercells using the open source PHONOPY software package [22] and fit the force constant data to compute the dynamical matrix.

IV. RESULTS AND DISCUSSION

A. Experimental results

1. X-ray diffraction

Initially, the crystal structure of the alloys is investigated using the standard powder XRD method with Cu-kα radiation. The observed Bragg reflection patterns clearly indicate that the alloys crystallize in the cubic structure. The quaternary Heusler alloys, XX′YZ exhibit LiMgPdSn-type structure whose primitive cell contains four atoms at the Wyckoff positions 4*a*, 4*b*, 4*c*, and 4*d*. The structure factor for the quaternary Heusler alloy with X at 4*b*, X′ at 4*c*, Y at 4*d*, and Z at 4*a* Wyckoff positions can be written as

$$F_{hkl} = 4\left(f_Z + f_Y e^{\pi i(h+k+l)} + f_X e^{\frac{\pi}{2}i(h+k+l)} + f_{X'} e^{\frac{-\pi}{2}i(h+k+l)}\right), \quad (1)$$

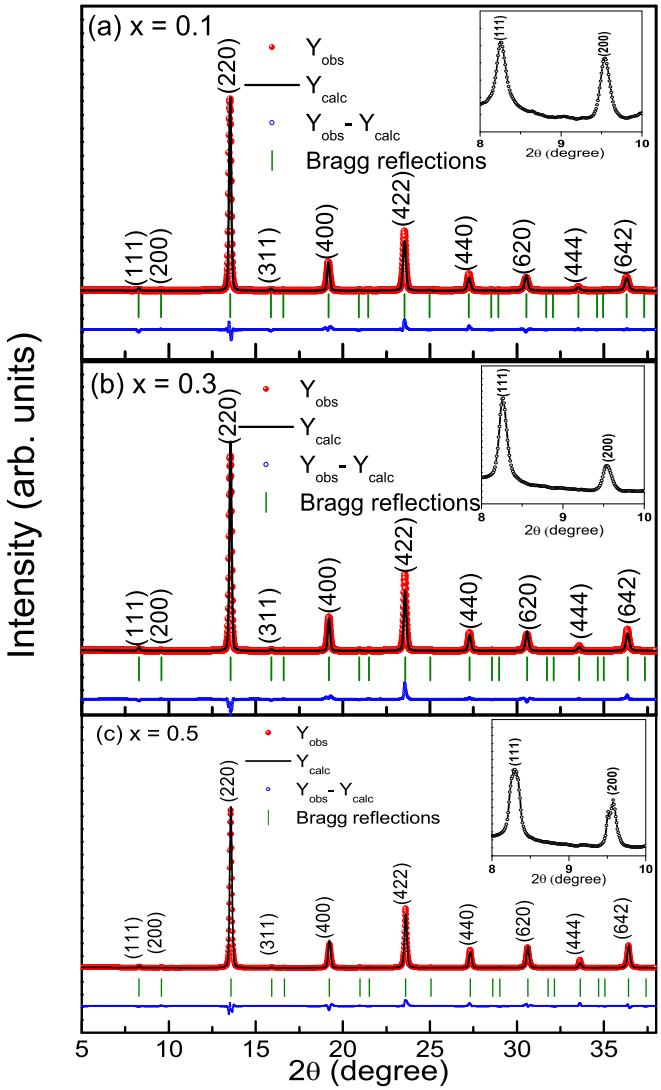

FIG. 2. Anomalous XRD patterns of $Co_{1+x}Fe_{1-x}CrGa$ ($x = 0.1$, 0.3, and 0.5) alloys. Y_{obs} and Y_{calc} are the observed and calculated scattered intensities. Insets in each plots show zoomed region in the vicinity of (111) and (200) peaks.

where f_X, $f_{X'}$, f_Y, and f_Z are the atomic scattering factors for X, X′, Y, and Z, respectively. The structure factor for the superlattice reflections can be written as

$$F_{111} = 4[(f_Y - f_Z) - i(f_X - f_{X'})], \quad (2)$$

$$F_{200} = 4[(f_Y + f_Z) - (f_X - f_{X'})]. \quad (3)$$

In the case of B2 disorder (Y and Z atoms are randomly distributed), the intensity of the (111) peak should reduce or disappear, as seen from Eq. (2). For a completely disordered structure, i.e., A2 type (all four atoms occupy random positions), both the superlattice peaks (111) and (200) should be absent. It is found that the Co substitution in place of Fe has not changed the crystal structure of the parent compound CoFeCrGa. The low-angle, order-dependent superlattice reflections (111) and (200) peaks, which are characteristics of a perfectly ordered Heusler structure, were not visible

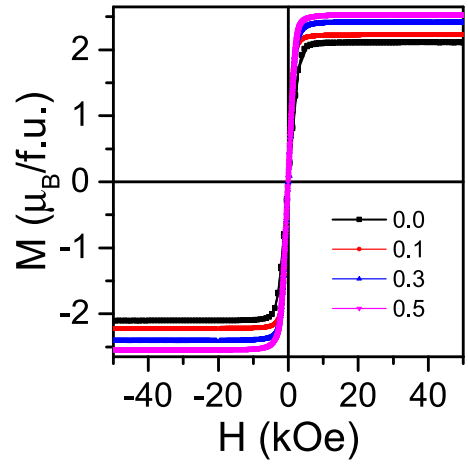

FIG. 3. Isothermal magnetization curves for $Co_{1+x}Fe_{1-x}CrGa$ alloys at 5 K.

in the standard XRD pattern. This could be due to antisite disorder (B2 type, DO_3, or A2 type) or the similar scattering factors of the constituent elements Co, Fe, Cr, and Ga. Due to the similar scattering factors of the constituent elements in $Co_{1+x}Fe_{1-x}CrGa$, standard powder XRD is not sufficient to determine the correct structure. Thus, in addition to the powder XRD, anomalous XRD patterns were obtained using the synchrotron radiation ($\lambda = 0.4815$ Å). Figure 2 shows the anomalous XRD patterns of $Co_{1+x}Fe_{1-x}CrGa$ alloys ($x = 0.1$, 0.3, and 0.5), recorded at room temperature. The superlattice reflections (111) and (200), which are not observed using the standard powder XRD method, are clearly visible in the anomalous XRD patterns (shown in the insets of Fig. 2). However, the intensity of the superlattice reflections is weak. The presence of both (111) and (200) peaks rule out the possibility of B2 and A2 disordered structures for these alloys. The earlier report on Mössbauer spectroscopy studies of CoFeCrGa alloy has confirmed the DO_3 disorder [8]. Thus, the alloys in the present investigation may have some amount of DO_3 disorder. The lattice parameters were found using Fullprof Suite software, assuming the Y-type ordering. The lattice parameters were found to be 5.782(1), 5.774(3),

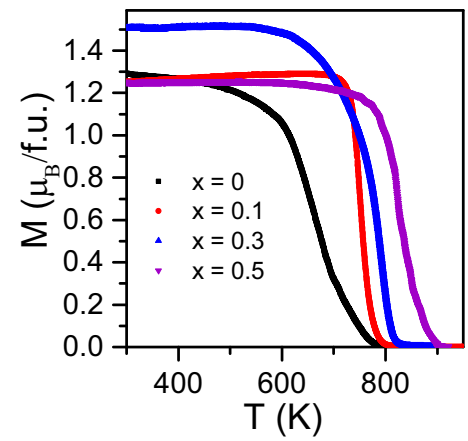

FIG. 4. Temperature dependence of magnetization in 500 Oe for $Co_{1+x}Fe_{1-x}CrGa$ alloys.

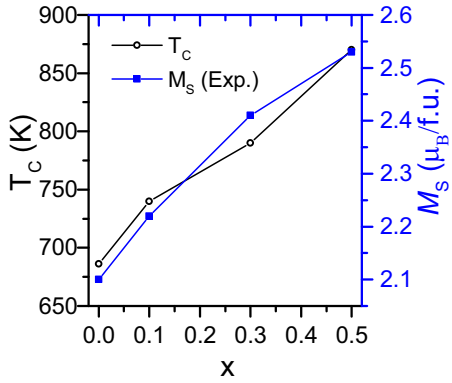

FIG. 5. Variation of Curie temperature (T_C) and experimental saturation magnetization with x for $Co_{1+x}Fe_{1-x}CrGa$ alloys. T_c is calculated from the minima of the first-order derivative of M vs T curve.

and 5.765(1) Å for $x = 0.1$, 0.3, and 0.5, respectively. Thus, substituting Fe by Co leads to only a marginal change in the lattice parameter.

2. Magnetic properties

Figure 3 shows the isothermal magnetization curves for $Co_{1+x}Fe_{1-x}CrGa$ ($x = 0$, 0.1, 0.3, and 0.5) alloys at 5 K. The almost negligible hysteresis shows the soft magnetic nature of the alloys. Heusler alloys are known to follow the Slater-Pauling rule [23,24], according to which the total moment per unit cell is given by

$$m = (N_v - 24)\mu_B, \tag{4}$$

where N_v is the number of valence electrons per unit cell.

Since the valance electronic configuration of Co, Fe, Cr, and Ga are $4s^2 3d^7$, $4s^2 3d^6$, $4s^1 3d^5$, and $4s^2 4p^1$, respectively, as per Slater-Pauling rule, the magnetic moment should increase from 2.1 μ_B/f.u. for $x = 0.1$ to 2.5 μ_B/f.u. for $x = 0.5$. The obtained experimental M_s values (at 5 K) are in fair agreement with those calculated using the Slater-Pauling rule.

Figure 4 shows the temperature dependence of the magnetization at a constant field of 500 Oe in the temperature range of 300–950 K for $Co_{1+x}Fe_{1-x}CrGa$ alloys. The Curie temperature was estimated by taking the minima of the first-order derivative of M–T curve. Figure 5 shows the Curie temperature vs x curve, which shows that the T_C increases almost linearly with x. It is found to be 686 K for $x = 0$ and 870 K for $x = 0.5$. The obtained T_C value for $x = 0.3$ (790 K) is found to be the highest among all previously reported SGS materials [9–11]. The high T_C makes these alloys better suited for spintronic applications in real-time devices.

3. Resistivity measurements: Longitudinal component

Figure 6 shows the measured temperature dependence of the longitudinal resistivity (ρ_{xx}) for $Co_{1+x}Fe_{1-x}CrGa$ alloys in zero field. The resistivity behavior in the temperature region from 5–350 K was investigated.

(i) $x = 0.1$, 0.2, 0.3, and 0.4.

As shown in Figs. 6(a) and 6(b), alloys with $x = 0.1$ and 0.3 show semiconducting behavior with a negative temperature coefficient ($d\rho/dT < 0$). A similar dependence was observed for $x = 0.2$ and 0.4. The temperature dependence of electrical conductivity σ_{xx} for $Co_{1+x}Fe_{1-x}CrGa$ ($x = 0.1$, 0.2, 0.3, and 0.4) is shown in Fig. 7 and it is clear that the alloys with $x = 0.1$ to 0.4 exhibit nonmetallic behavior; σ_{xx} increases with increasing temperature. The σ_{xx} vs T behavior is different from that of conventional metals or semiconductors as they exhibit exponential decrease or increase in the conductivity. A similar kind of behavior is also reported for the parent alloy CoFeCrGa [8]. Thus, the σ_{xx} vs T behavior gives an indication of SGS nature in these alloys. The value of $\sigma_{xx}(T)$ at 300 K lies in the range 2290 S cm^{-1} to 3294 S cm^{-1} and is close to that of other reported SGS materials [8,9]. To further analyze this behavior, $\sigma_{xx}(T)$ is described by a two-carrier model [11,25,26] in the temperature range $T = 100$ to 350 K. In this model, the total conductivity is given by

$$\frac{1}{\rho_{xx}} = \sigma_{xx}(T) = e(n_e\mu_e + n_h\mu_h), \tag{5}$$

where the first and second terms correspond to the electronic and hole components, respectively. The mobilities are given by $\mu_i = \frac{1}{\alpha_i T + \beta_i}$ where $i =$ e or h. Here, the α term corresponds to electron phonon scattering and the β term results from the mobility due to defects at $T = 0$ K. The fit assumes that the number of carriers is given by $n_e \sim n_{e0}\exp(-\Delta E_e/k_B T)$ and $n_h \sim n_{ho}\exp(-\Delta E_h/k_B T)$, where ΔE_i are the gaps for the carriers. Thus, under these assumptions, the conductivity can

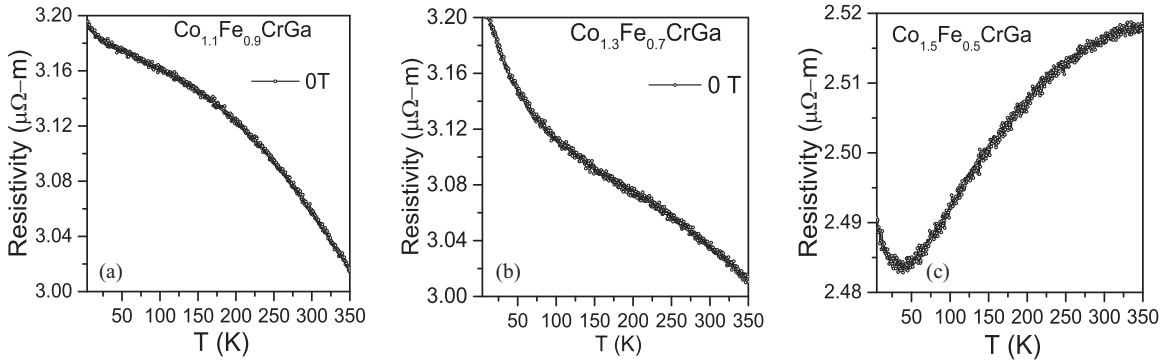

FIG. 6. Temperature dependence of electrical resistivity(ρ) for $Co_{1+x}Fe_{1-x}CrGa$ alloys in zero field.

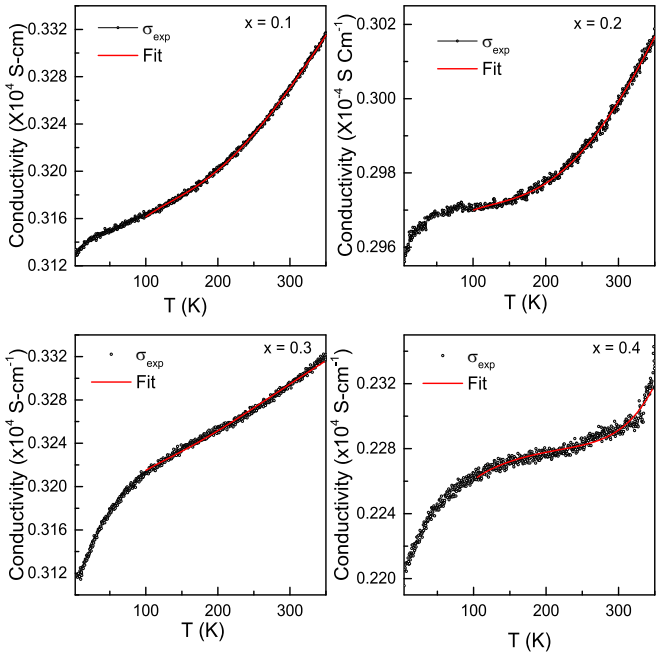

FIG. 7. Variation of electrical conductivity with temperature in zero field along with the fit [using Eq. (6)] shown by red line (above 100 K) using two carrier model for $Co_{1+x}Fe_{1-x}CrGa$ ($x = 0.1$, 0.2, 0.3, and 0.4).

now be written as

$$\sigma_{xx}(T) = A(T)\exp(-\Delta E_e/K_BT) + B(T)\exp(-\Delta E_h/K_BT), \tag{6}$$

where $A(T) = \frac{en_{e0}\mu_{e0}}{1+\alpha'_eT}$ and $B(T) = \frac{en_{h0}\mu_{h0}}{1+\alpha'_hT}$.

Fitting to this model (red solid curves in Fig. 7) gives the temperature coefficients $\alpha'_e \sim 0$ and $\alpha'_h \sim 0$, which suggest that in these alloys the mobility is mainly due to defect scattering instead of phonons. The gaps $\Delta E_e(\Delta E_h)$ are found to be 76.2 meV (0.1), 89.5 meV (0.1), and 53.5 meV (0.1) for $x = 0.1$, 0.2, and 0.3, respectively. Here, the low gaps are associated with holes since from the Hall measurement (see Fig. 8), it is found that holes are the majority carriers.

(ii) $x = 0.5$.

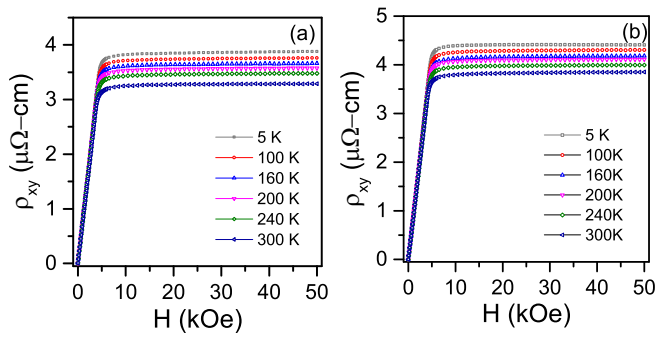

FIG. 8. Hall resistivity (ρ_{xy}) as a function of magnetic field (H), measured at different temperatures for (a) $Co_{1.1}Fe_{0.9}CrGa$ and (b) $Co_{1.3}Fe_{0.7}CrGa$.

For $x = 0.5$, the resistivity is found to increase with temperature and thus shows the metallic behavior [Fig. 6(c)]. A minimum in the resistivity with an upturn is observed in this alloy. Such behavior is observed in some other HM Heusler alloys [27,28] as well and is generally ascribed to a weak localization mechanism, i.e., the disorder augmented coherent backscattering of conduction electrons [29]. Thus, transition from SGS to HM behavior is expected when 50% Fe is replaced by Co in CoFeCrGa.

4. Anomalous Hall effect measurements

For a ferromagnet, in addition to the ordinary Hall effect (OHE), the transverse resistivity has a contribution from the magnetization as well, known as anomalous Hall resistivity. This additional transverse voltage (known as AHE) is due to the asymmetric scattering of current carrying electrons. Thus, in such a material, the transverse resistivity ρ_{xy} is written as the sum of ordinary Hall resistivity ρ_{xy}^{OHE} and the anomalous Hall resistivity ρ_{xy}^{s} [30],

$$\rho_{xy}(T) = \rho_{xy}^{OHE} + \rho_{xy}^{s} = R_0H + R_{AHE}M, \tag{7}$$

where ρ_{xy}^{OHE} is written as the product of ordinary Hall coefficient R_0 and the applied magnetic field and ρ_{xy}^{s} is written as the product of anomalous Hall coefficient R_{AHE} and magnetization. The ordinary Hall coefficient R_0 depends on the types of carriers (electrons or holes) and their density and is inversely related to the product of the carrier concentration and the electron charge. In lower fields, the measured Hall resistivity is dominated by the AHE, while the effect of OHE typically appears in the higher fields.

The Hall resistivity(ρ_{xy}) curves as a function of magnetic field were recorded at various temperatures in the field range of 0 to 50 kOe. Figure 8 shows the ρ_{xy} versus H curves at 5K, 20 K, 100 K, 160 K, 200 K, 240 K, and 300 K for $x = 0.1$ and 0.3. In the low field regime, ρ_{xy} is found to increase with an increase in magnetic field (dominated by AHE) and gets saturated in the higher field regime. The Hall resistivity shows similar behavior as observed for the magnetization isotherms (see Fig. 3). The AHE contribution in ρ_{xy} (i.e., ρ_{AHE}) is calculated by extrapolating the high field data toward the zero field since the AHE contribution is typically high and saturates at high fields. Figure 9 shows the Hall conductivity (σ_{xy}) versus H curves for $x = 0.1$ and 0.3. The anomalous Hall conductivity value, σ_{xy0} at 5 K is found to be 38 S cm^{-1} and 43 S cm^{-1} for $x = 0.1$ and 0.3, respectively. These values are close to that of the other reported SGS Heusler systems [10] and much smaller than those of HM Heusler systems [31]. Figures 10(a) and 11(a) show the temperature dependence of extracted ρ_{AHE} for $x = 0.1$ and 0.3, respectively, and it is seen that it increases as the temperature is reduced. This behavior is similar to that observed for longitudinal resistivity $\rho_{xx}(T)$ (see Fig. 6).

The AHE generally has two components: intrinsic and extrinsic [30]. The intrinsic component is caused by the transverse velocity of Bloch electrons in ideal magnetic crystal and depends only on the band structure. The mechanism of intrinsic contribution to AHE was first proposed by Karplus and Luttinger [32] and later it was redeveloped in terms of Berry's phase [33]. The extrinsic mechanism is due to the

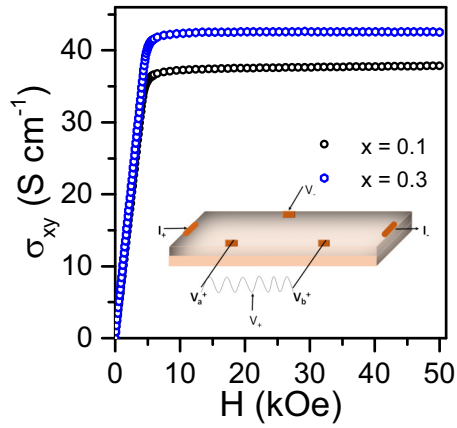

FIG. 9. Hall conductivity σ_{xy} versus applied field for $Co_{1+x}Fe_{1-x}CrGa$ ($x = 0.1$ and 0.3) at 5 K.

spin-orbit coupling-induced asymmetric scattering of electrons near impurity sites which give rise to two contributions (i) Skew scattering [34] and (ii) side-jump scattering [35]. To estimate the intrinsic and extrinsic AHE contributions, a scaling model reported by Tian *et al.* [36] is used, according to which

$$\rho_{\mathrm{AHE}} = \alpha\rho_{xx0} + \beta\rho_{xx0}^2 + b\rho_{xx}^2 \tag{8}$$

Combining the temperature independent terms, the above equation can be written as

$$\rho_{\mathrm{AHE}} = a'\rho_{xx0} + b\rho_{xx}^2, \tag{9}$$

where $a' = \alpha + \beta\rho_{xx0}$ and represents the extrinsic contribution due to skew and side jump impurity scattering whereas, b is the intrinsic parameter. The variation of ρ_{xy} with ρ_{xx}^2 along with the fit to Eq. (9) (blue solid curve) for $x = 0.1$ and 0.3 is shown in Figs. 10(b) and 11(b), respectively. The fitted value of a' is -10^{-2} and -1.5×10^{-2} for $x = 0.1$ and 0.3, respectively. The value of b which gives the temperature-independent intrinsic contribution to ρ_{AHE} is found to increase from 69 S cm^{-1} to 94 S cm^{-1} as x changes from $x = 0.1$ to 0.3.

Using the relation, $\sigma_{xy} \approx \rho_{xy}/\rho_{xx}^2$, we can calculate the anomalous Hall conductivity σ_{AH} and also Eq. (9) in terms of conductivity can be written as

$$\sigma_{\mathrm{AHE}} = \sigma_{\mathrm{AHE}}^{\mathrm{int}} + \sigma_{\mathrm{AHE}}^{\mathrm{ext}} = b + a'\sigma_{xx0}^{-1}\sigma_{xx}^2, \tag{10}$$

where, $\sigma_{\mathrm{AHE}}^{\mathrm{int}}$ and $\sigma_{\mathrm{AHE}}^{\mathrm{ext}}$ represent the intrinsic and extrinsic contributions to the total anomalous Hall conductivity σ_{AHE}. Here, $\sigma_{xx0} = 1/\rho_{xx0}$ and $\sigma_{xx}^2 = 1/\sigma_{xx}^2$ are the residual and longitudinal conductivity, respectively. It is important to note that the first term $\sigma_{\mathrm{AHE}}^{\mathrm{int}}$ is the Karplus-Luttinger term which originates from the Berry curvature and the second term $\sigma_{\mathrm{AHE}}^{\mathrm{ext}}$ is the sum of extrinsic effects, i.e., $\sigma_{\mathrm{AHE}}^{\mathrm{ext}} = \sigma^{ss} + \sigma^{sj}$, where σ^{ss} and σ^{sj} represent the extrinsic skew scattering and side jump scattering, respectively [36]. Figures 10(c) and 11(c) show the temperature dependence of $|\sigma_{\mathrm{AHE}}^{\mathrm{ext}}|$, where $\sigma_{\mathrm{AHE}}^{\mathrm{ext}}$ includes both extrinsic effects (skew scattering and side jump scattering). The finite $\sigma_{\mathrm{AHE}}^{\mathrm{int}}$ confirms the nonzero Berry curvature in these alloys. The increase in the value of intrinsic parameter b with x implies an increase in the scattering independent contribution and is attributed to the improved chemical ordering within the lattice [37]. The negative value of extrinsic parameter a' indicates that the extrinsic contribution due to skew symmetric and the side jump scattering contributed to the σ_{AHE} in the opposite way as the intrinsic Karplus-Luttinger term does.

5. Seebeck coefficient and heat capacity measurements

Figure 12 shows the temperature dependence of Seebeck coefficient for $Co_{1.1}Fe_{0.9}CrGa$ and $Co_{1.3}Fe_{0.7}CrGa$ alloys. The alloys exhibit positive Seebeck coefficient which indicates that the majority carriers are of hole type (also confirmed from Hall measurements). The Seebeck coefficient for $x = 0.1$ (0.3) is negligibly small (nearly zero) in the temperature range from 2 to 40 K (2 to 25 K), which may be attributed to the electron and hole compensation and for $40 < T < 300$ K, it has a very low value of 1.1 μV/K (2.2 μV/K). This behavior is different from that of regular semiconductors, since they are known to have high Seebeck coefficient values ($\sim$200 – 300 μV/K). A similar dependence as seen in the present case was also observed for Mn_2CoAl, another SGS material, from the Heusler family [10]. This feature again supports the SGS behavior in these alloys.

Heat capacity measurements were also performed for two alloys $x = 0.1$ and $x = 0.3$. In general, the heat capacity can be expressed as the sum of electronic, lattice, and magnetic contributions. But at low temperatures, the magnetic

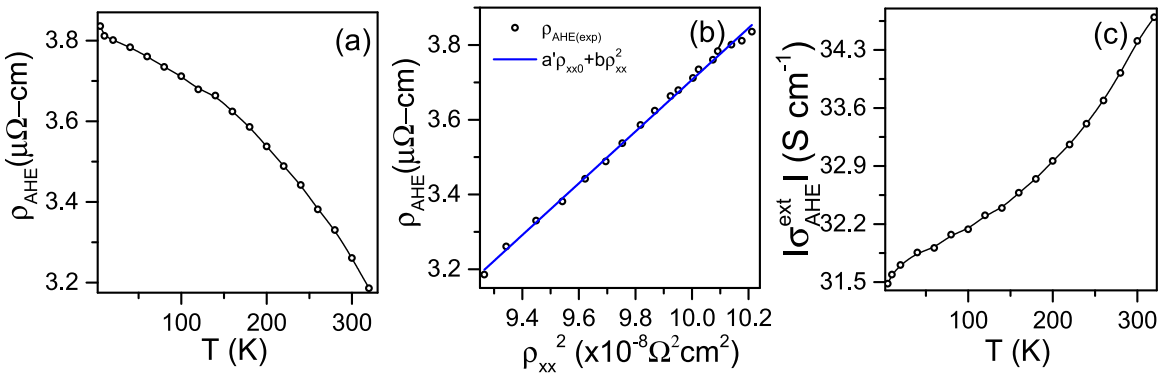

FIG. 10. The variation of (a) ρ_{AHE} with temperature, (b) ρ_{AHE} with ρ_{xx}^2 with the fitted curve (blue) using Eq. (9), and (c) extrinsic contribution of σ_{AHE} with temperature for $Co_{1.1}Fe_{0.9}CrGa$ alloys.

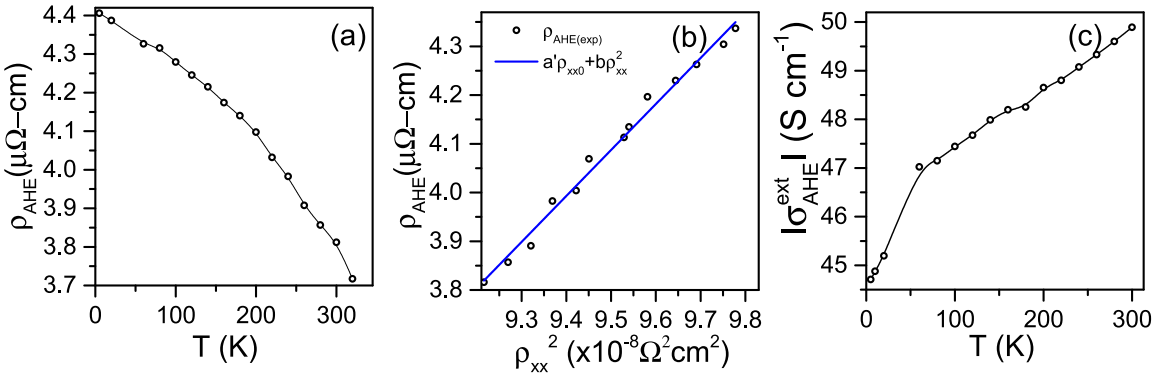

FIG. 11. The variation of (a) ρ_{AHE} with temperature, (b) ρ_{AHE} with ρ_{xx}^2 with the fitted curve (blue) using Eq. (9), and (c) extrinsic contribution σ_{AHE} with temperature for $Co_{1.3}Fe_{0.7}CrGa$ alloys.

excitations have insignificant contribution to the total heat capacity and the other two contributions becomes dominant. Thus, at low temperatures, the heat capacity of a ferromagnetic material can be described by the Sommerfeld-Debye model [38], according to which

$$C(T) = \gamma T + \beta T^3, \tag{11}$$

where the first and second terms represent the electronic and lattice contributions to the total heat capacity, respectively. Here, γ is the Sommerfeld coefficient representing the electronic part and β is the lattice coefficient. Figure 13 shows the temperature dependence of heat capacity (C/T vs T^2) for $x = 0.1$ (left) and $x = 0.3$ (right) concentration. The inset shows the C vs T plot in zero field. Evidently, C/T vs T^2 shows a linear behavior, and as such the slope and the intercept of the curve correspond to the value of γ and β of Eq. (11), respectively. In the free electron model, the value of γ corresponds to the density of states at the Fermi level according to the relation [39]

$$N(E_F) = \frac{3\gamma}{\pi^2 N_A {k_B}^2}, \tag{12}$$

where N_A is the Avogadro number and k_B is the Boltzmann constant.

From the value of β, the Debye temperature can be calculated using the following relation [39]:

$$\theta_D = \frac{234ZR}{\beta}, \tag{13}$$

where R is the universal gas constant and Z is the number of atoms per formula unit.

A fitting of C/T vs T^2 curve with Eq. (11) gives $\gamma = 18\,\text{mJmole}^{-1}\text{K}^{-2}$ and $\beta = 0.1\,\text{mJmole}^{-1}\text{K}^{-4}$ for $x = 0.1$. For $x = 0.3$, the obtained values of γ and β are 13 $\text{mJmole}^{-1}\text{K}^{-2}$ and 0.12 $\text{mJmole}^{-1}\text{K}^{-4}$, respectively. The calculated value of density of states $N(E_F)$ from the extracted Sommerfeld constant for $x = 0.1$ and 0.3 is found to be 1.9 and 1.4 states $\text{eV}^{-1}\text{f.u.}^{-1}$, respectively. The value of θ_D is found to be 426 K and 405 K for$x = 0.1$ and 0.3, respectively. It should be noted that these estimates for $N(E_F)$ and θ_D are purely based on the free electron model and they only guide us to facilitate a qualitative trend.

B. Theoretical results

1. Electronic structure

According to the experimental analysis, $Co_{1+x}Fe_{1-x}CrGa$ ($x = 0.1$ to 0.5) crystallizes in LiMgPdSn-type structure having space group $F\bar{4}3m$ (number of 216). To obtain the electronic density of states (DOS) for a desired x, a fully optimized $2 \times 2 \times 2$ supercell which corresponds to a minimum ground-state energy has been used.

Figure 14 shows the electronic DOS for majority and minority spin channels for $Co_{1+x}Fe_{1-x}CrGa$ at $x = 0$, 0.125, 0.25, 0.375, and 0.5. At $x = 0$, i.e., there is no excess of Co, the alloy shows almost vanishing DOS in one spin channel

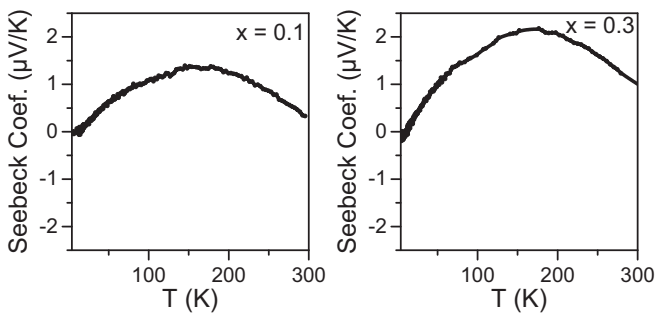

FIG. 12. Variation of Seebeck coefficient with temperature for $Co_{1.1}Fe_{0.9}CrGa$ and $Co_{1.3}Fe_{0.7}CrGa$ alloys.

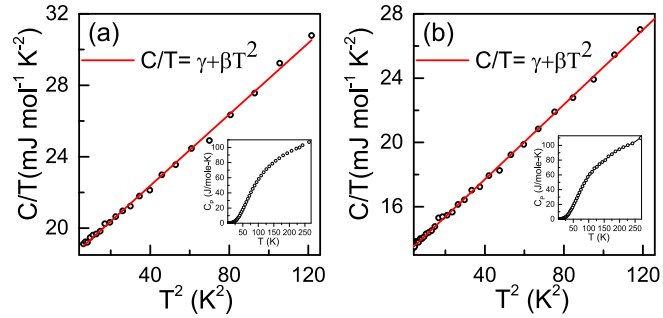

FIG. 13. Heat capacity (C/T) vs T^2 plot for (a) $Co_{1.1}Fe_{0.9}CrGa$ and (b) $Co_{1.3}Fe_{0.7}CrGa$, in low temperature range. Insets shows the C vs T curve for high T range, up to 250 K.

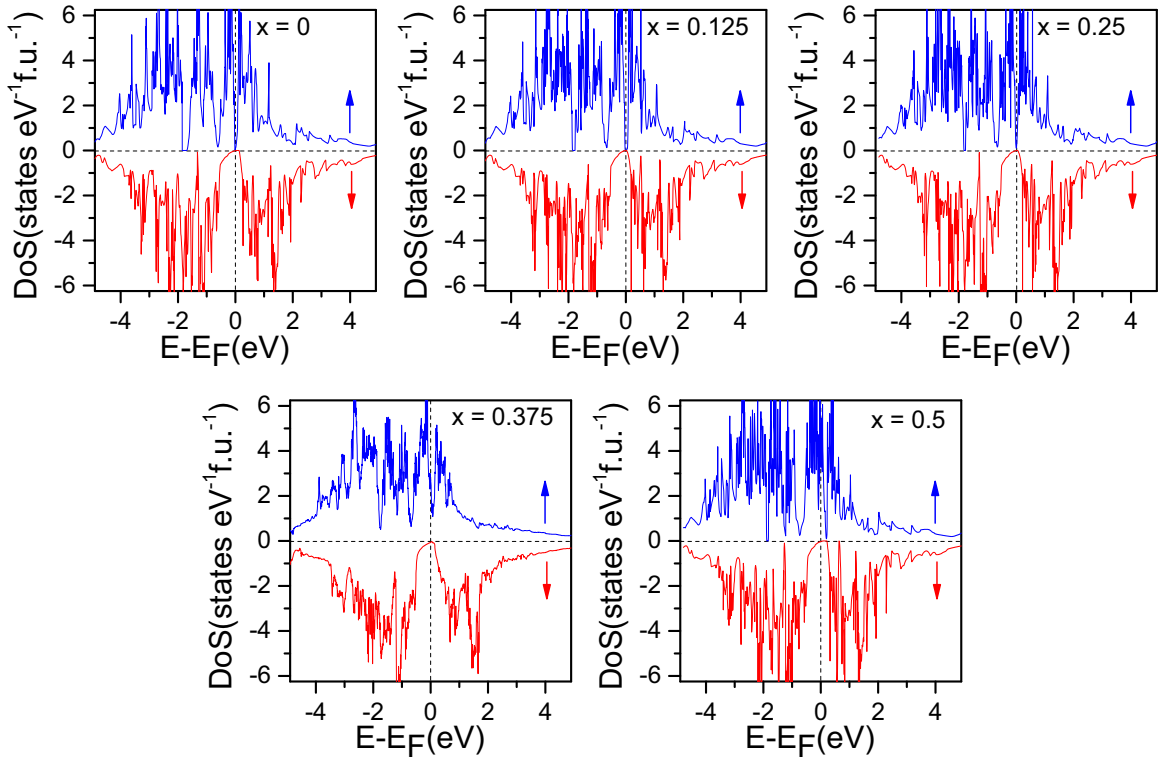

FIG. 14. Spin polarized density of states for $Co_{1+x}Fe_{1-x}CrGa$ at different x's.

and finite gap in the other spin channel, concluding it to be SGS. The spin-gapless behavior is retained in the system for $x < 0.375$ and the alloy becomes HM for $x \geqslant 0.375$ although there are small states at the Fermi level in the spin down channel, but the magnitude of this is negligibly small. The calculated value of total magnetic moment per formula unit matches fairly with the Slater-Pauling value for different x's, as shown in Table I.

2. Phonon dispersion

Phonon dispersion of the alloys, $Co_{1+x}Fe_{1-x}CrGa$ with various x values, has been shown in Fig. 15. There are 32 atoms in the considered unit cell, which generate three acoustic modes and ($3n$-3 = 93) optical modes, where n is the number of atoms present in the unit cell. We have not observed any imaginary (or soft vibrational modes) frequencies in the whole range of Brillouin zone, which supports thermal stability of the alloys, although it is not obvious from the figure, but the degeneracy of the transverse optical (TO) and longitudinal optical (LO) phonons at Γ point is broken, giving rise to the so-called LO-TO splitting. This mainly arises due to the long-range nature of the Coulomb interaction. The calculated frequency of the optical modes for $Co_{1+x}Fe_{1-x}CrGa$ (for all x) lie within 3.34 THz to 8.67 THz at Γ point. One interesting feature of the phonon dispersion is that some of the optical branches are coupled with the acoustic branches at high symmetry points. This is because of the comparable masses of the constituent elements. The atomic mass of Co, Fe, Cr, and Ga is 58.933 amu, 55.845 amu, 51.996 amu, and 69.723 amu respectively.

TABLE I. Comparison between Slater-Pauling and calculated values of saturation magnetization (μ_B/f.u.) for $Co_{1+x}Fe_{1-x}CrGa$ alloys.

x	$M_S(SP)$	$M_S(Calc.)$
0.0	2.00	2.01
0.125	2.125	2.14
0.25	2.25	2.25
0.375	2.375	2.377
0.5	2.50	2.51

V. SUMMARY AND CONCLUSION

In conclusion, the quaternary Heusler alloys $Co_{1+x}Fe_{1-x}CrGa$ are found to show promising properties for spintronic applications. The alloys are found to crystallize in Y-type Heusler structure. The saturation magnetization is found to be in fair agreement with the value predicted by Slater-Pauling rule, which is a prerequisite for spintronic materials. The transition temperature is found to increase with x and lies above room temperature (690 K to 870 K). Resistivity measurements confirm the semiconducting behavior for $x \leqslant 0.4$ and metallic behavior for $x = 0.5$. However, the absence of exponential dependence of resistivity on temperature indicates the semiconducting nature, but with spin gapless behavior for $x \leqslant 0.4$. The alloy with $x = 0.5$ shows metallic nature with a minima in resistivity, which is associated with the weak localization effect. Ordinary and anomalous Hall contributions have been separated and the intrinsic and extrinsic contribution of the later are also identified. The intrinsic contribution is found to increase as

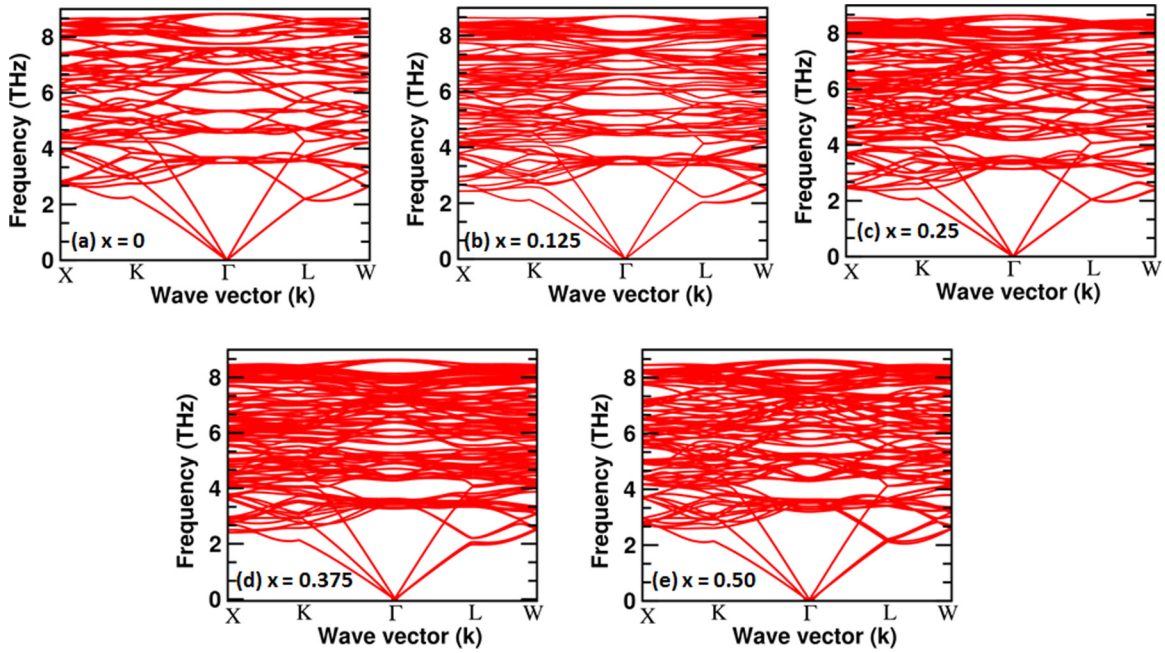

FIG. 15. Phonon dispersion of $Co_{1+x}Fe_{1-x}CrGa$ at different x's.

x increases and is correlated with the improved chemical ordering within the lattice. The extrinsic contribution is found to be negative and thus contributes to the AHE in the opposite way as the Karplus-Luttinger term does. The conductivity value (σ_{xx}) at 300 K lies in the range of 2289 S cm^{-1} to 3294 S cm^{-1}, which is close to other reported SGS materials. The order of magnitude of anomalous Hall conductivity (σ_{AHE}) is found to be similar to the other SGS material. The negligible Seebeck coefficient along with the conductivity behavior also supports the SGS nature. Thus, we conclude, on the basis of experiment and theory, that $Co_{1+x}Fe_{1-x}CrGa$ series show SGS nature up to $x = 0.4$, beyond which it is HMF. The obtained T_C value for $x = 0.3$ (790 K) is found to be the highest among all the previously reported SGS materials.

ACKNOWLEDGMENTS

D.R. would like to thank Council of Scientific and Industrial Research (CSIR), India for providing a senior research fellowship. D.R. thanks Dr. V. K. Kushwaha for helping in Seebeck coefficient measurements. D.R. also thanks Dr. Velaga Srihari, ECXRD beamline, BL-11, Indus-2, RRCAT for carrying out synchrotron XRD measurements.

[1] I. M. Tsidilkovski, *Electron Spectrum of Gapless Semiconductors*, edited by K. von Klitzing, Springer Series in Solid-State Sciences, Vol. 116 (Springer, New York, 1997).
[2] L. Wang and Y. Jin, J. Magn. Magn. Mater. **385**, 55 (2015).
[3] M. Wang, R. P. Campion, A. W. Rushforth, K. W. Edmonds, C. T. Foxon, and B. L. Gallagher, Appl. Phys. Lett. **93**, 132103 (2008).
[4] G. Z. Xu, E. K. Liu, Y. Du, G. J. Li, G. D. Liu, W. H. Wang, and G. H. Wu, Europhys. Lett. **102**, 17007 (2013).
[5] S. Skaftouros, K. Özdoğan, E. Šašioğlu, and I. Galanakis, Appl. Phys. Lett. **102**, 022402 (2013).
[6] H. Y. Jia, X. F. Dai, L. Y. Wang, R. Liu, X. T. Wang, P. P. Li, Y. T. Cui, and G. D. Liu, AIP Adv. **4**, 047113 (2014).
[7] X. L. Wang, Phys. Rev. Lett. **100**, 156404 (2008).
[8] L. Bainsla, A. I. Mallick, M. M. Raja, A. A. Coelho, A. K. Nigam, D. D. Johnson, A. Alam, and K. G. Suresh, Phys. Rev. B **92**, 045201 (2015).
[9] L. Bainsla, A. I. Mallick, M. M. Raja, A. K. Nigam, B. S. D. C. S. Varaprasad, Y. K. Takahashi, A. Alam, K. G. Suresh, and K. Hono, Phys. Rev. B **91**, 104408 (2015).
[10] S. Ouardi, G. H. Fecher, C. Felser, and J. Kübler, Phys. Rev. Lett. **110**, 100401 (2013).
[11] Y. Venkateswara, S. Gupta, S. S. Samatham, M. R. Varma, Enamullah, K. G. Suresh, and A. Alam, Phys. Rev. B **97**, 054407 (2018).
[12] A. P. Hammersley, S. O. Svensson, M. Hanfland, A. N. Fitch, and D. Hausermann, High Press. Res. **14**, 235 (1996).
[13] https://www.ill.eu/sites/fullprof/php/tutorials.html.
[14] P. Hohenberg and W. Kohn, Phys. Rev. **136**, B864 (1964).
[15] G. Kresse and J. Furthmüller, Phys. Rev. B **54**, 11169 (1996).
[16] G. Kresse and J. Furthmüller, Comp. Mater. Sci. **6**, 15 (1996).
[17] G. Kresse and J. Hafner, Phys. Rev. B **47**, 558 (1993).
[18] G. Kresse and D. Joubert, Phys. Rev. B **59**, 1758 (1999).
[19] J. P. Perdew, K. Burke, and M. Ernzerhof, Phys. Rev. Lett. **77**, 3865 (1996).
[20] S. Baroni, S. de Gironcoli, A. Dal Corso, and P. Giannozzi, Rev. Mod. Phys. **73**, 515 (2001).
[21] X. Gonze and C. Lee, Phys. Rev. B **55**, 10355 (1997).
[22] A. Togo, F. Oba, and I. Tanaka, Phys. Rev. B **78**, 134106 (2008).

[23] I. Galanakis, P. H. Dederichs, and N. Papanikolaou, Phys. Rev. B **66**, 174429 (2002).
[24] D. Rani, Enamullah, K. G. Suresh, A. K. Yadav, S. N. Jha, D. Bhattacharyya, M. R. Varma, and A. Alam, Phys. Rev. B **96**, 184404 (2017).
[25] M. E. Jamer, B. A. Assaf, T. Devakul, and D. Heiman, Appl. Phys. Lett. **103**, 142403 (2013).
[26] M. E. Jamer, Y. J. Wang, G. M. Stephen, I. J. McDonald, A. J. Grutter, G. E. Sterbinsky, D. A. Arena, J. A. Borchers, B. J. Kirby, L. H. Lewis, B. Barbiellini, A. Bansil, and D. Heiman, Phys. Rev. Appl. **7**, 064036 (2017).
[27] J. C. Prestigiacomo, D. P. Young, P. W. Adams, and S. Stadler, J. Appl. Phys. **115**, 043712 (2014).
[28] D. Rani, J. Kangsabanik, K. G. Suresh, N. Patra, D. Bhattacharyya, S. N. Jha, and A. Alam, Phys. Rev. Appl. **10**, 054022 (2018).
[29] P. A. Lee and T. V. Ramakrishnan, Rev. Mod. Phys. **57**, 287 (1985).
[30] N. Nagaosa, J. Sinova, S. Onoda, A. H. MacDonald, and N. P. Ong, Rev. Mod. Phys. **82**, 1539 (2010).
[31] D. Bombor, C. G. F. Blum, O. Volkonskiy, S. Rodan, S. Wurmehl, C. Hess, and B. Büchner, Phys. Rev. Lett. **110**, 066601 (2013).
[32] R. Karplus and J. M. Luttinger, Phys. Rev. **95**, 1154 (1954).
[33] G. Sundaram and Q. Niu, Phys. Rev. B **59**, 14915 (1999).
[34] J. Smit, Physica **24**, 39 (1958).
[35] L. Berger, Phys. Rev. B **2**, 4559 (1970).
[36] Y. Tian, L. Ye, and X. Jin, Phys. Rev. Lett. **103**, 087206 (2009).
[37] L. J. Zhu, D. Pan, and J. H. Zhao, Phys. Rev. B **89**, 220406(R) (2014).
[38] J. W. Simonson, D. Wu, W. J. Xie, T. M. Tritt, and S. J. Poon, Phys. Rev. B **83**, 235211 (2011).
[39] R. Y. Umetsu, X. Xu, W. Ito, and R. Kainuma, Metals **7**, 414 (2017).